Dhar, Prodyut; Etula, Jarkko; Bankar, Sandip Balasaheb

In Situ Bioprocessing of Bacterial Cellulose with Graphene

Published in:
ACS Applied Bio Materials

DOI:
10.1021/acsabm.9b00581

Published: 01/01/2019

Document Version
Publisher's PDF, also known as Version of record

Please cite the original version:
Dhar, P., Etula, J., & Bankar, S. B. (2019). In Situ Bioprocessing of Bacterial Cellulose with Graphene: Percolation Network Formation, Kinetic Analysis with Physicochemical and Structural Properties Assessment. *ACS Applied Bio Materials*. https://doi.org/10.1021/acsabm.9b00581

ACS APPLIED BIO MATERIALS
Article
Cite This: ACS Appl. Bio Mater. 2019, 2, 4052−4066
www.acsabm.org

In Situ Bioprocessing of Bacterial Cellulose with Graphene: Percolation Network Formation, Kinetic Analysis with Physicochemical and Structural Properties Assessment

Prodyut Dhar,*[†,‡] Jarkko Etula,[§] and Sandip Balasaheb Bankar*[†]

[†]Department of Bioproducts and Biosystems, School of Chemical Engineering, Aalto University, P.O. Box 16100, FI-000076, Aalto, Finland

[‡]Division of Forest and Biomaterials Science, Kyoto University, Kyoto 606-8502, Japan

[§]Department of Chemistry and Materials Science, School of Chemical Engineering, Aalto University, P.O. Box 16100, FI-000076, Aalto, Finland

Supporting Information

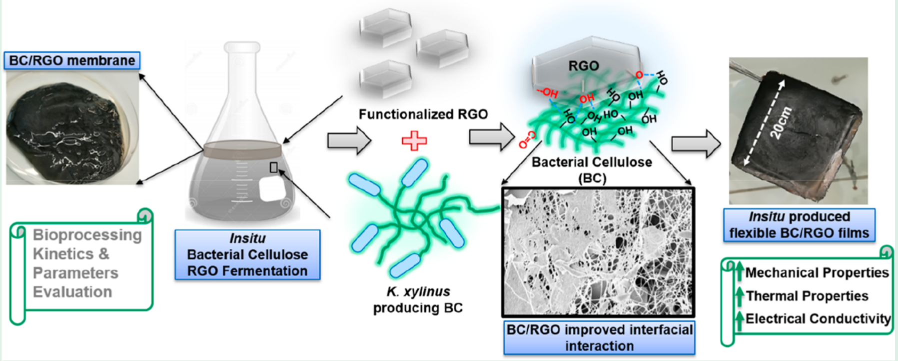

ABSTRACT: The understanding of microbial growth dynamics during *in situ* fermentation and production of bacterial cellulose (BC) with impressive properties mimicking artificial nacre, suitable for commodity applications remains fundamentally challenging. Fabrication of BC/graphene films through a single step *in situ* fermentation with improved properties provides a sustainable replacement to the conventional chemical-based modification using toxic compounds. This work reports the effect of reduced graphene oxide (RGO) on *in situ* fermentation kinetics and demonstrates the formation of percolated-network in BC/RGO nanostructures. The evaluation of kinetic parameters shows that the specific growth rate reaches optimal values at 3 wt % RGO loadings, with mixed growth associated BC production behavior. The two-dimensional graphene sheets uniformly dispersed into a three-dimensional matrix of BC nanofibers via hydrogen-bonded interactions along with *in situ* reductions of RGO sheets, as confirmed from spectroscopic studies. This study also demonstrates the presence of percolated network-like structures between BC fibers and RGO platelets, which resulted in the formation of nanostructures with exceptional mechanical robustness and electrical conductivity. The physicochemical and structural properties of fabricated BC/RGO films were found to significantly depend upon the RGO compositions as well as fermentation conditions. We envision that the proposed ecofriendly and scalable technology for the formation of BC/RGO films with excellent inherent properties and performance will attract great interest for its prospective applications in flexible electronics.

KEYWORDS: *bacterial cellulose, in situ fermentation, fermentation kinetics, structural properties, electrical conductivity*

INTRODUCTION

Bacterial cellulose (BC) is a microbially derived biopolymer which has recently attracted great attention from both academia as well as industrial researchers. BCs offers unique physicochemical or structural properties and have potential application in numerous fields. BC is a linear polysaccharide of glucan chains $(C_6H_{10}O_5)_n$, which consists of fibrils of nanodimensions (<100 nm) that are arranged to form a three-dimensional network.[1] BCs are also known to be the purest form of cellulose, with high crystallinity, mechanical properties, and biocompatibility compared to plant-derived cellulose. Thus, its applications in areas like biomedical engineering have been growing over the years.[2] Until today, BC has been used extensively in the medical technology directly as artificial skins for wound dressing,[3] as scaffolds for regeneration of tissues,[4] burn treatments, artificial blood vessels, and vascular grafts.[5] Unmodified BCs have high porosity and water absorption capabilities due to which they

Received: June 30, 2019
Accepted: August 2, 2019
Published: August 2, 2019

DOI: 10.1021/acsabm.9b00581

lack structural integrity under hydrophilic conditions that limit their engineering applications. However, to overcome such limitations, BC composites due to their high hydroxyl functionality maybe modified via *in situ* or *ex situ* based approaches.[6] BC modifications through silylation, esterification, carboxylation, quaternary ammonium salts, and ionic liquids (IL) are some of the well-known approaches recently reported in the literature.[6] Chemical-based approaches for BC modifications require its disintegration after fermentation, followed by treatment with toxic chemicals which poses issues, like reduced biocompatibility and nonbiodegradability. However, advancements in composite synthesis through newer techniques such as *in situ* BC modification have been recently developed which provide a single-step approach for nanocomposite fabrication with tailored properties.[7] Many *in situ* BC modifications have been focused on the development of nanocomposites with potential applications in tissue engineering,[8] electronics as free-standing electrodes or supercapacitors,[9] and water purification membranes or adsorbents.[10] Nonetheless, the proposed *in situ* fabrication of BC composites has shown some fundamental challenges such as lower BC yields, variability in BC production and variation in properties with batch and agglomeration of fillers,[9] as well as scalability issues. This might be due to the harsh environmental conditions and oxygen limitations during the growth of cellulose pellicles that hold the nano/microfillers in its network. Therefore, studies evaluating the microbial growth kinetics profile under various concentrations of micro/nanofillers as well as other biochemical parameters which might affect the cellulose biosynthesis need to be investigated to address the current challenges.

Many reported studies using biochemical routes for fabrication of BC composites utilize carbon-based nanomaterials such as graphene oxide,[10] carbon nanotubes,[8] and polyaniline[9] as fillers through *in situ* fermentation and layer by layer assembly techniques. The fabricated nanocomposites show improved strength, high surface area, and porosity which resulted in their potential application as adsorbents, supercapacitors, and hybrid scaffolds. Graphene oxide contains high hydroxyl and carboxyl functional groups but retains poor conductivity, due to which it is reduced to form structures resembling graphene but with trace quantities of oxygen and defects. Reduced graphene oxides (RGOs) are single-layered sheets with sp^2-hybridized carbon atoms and honeycomblike structure which have found tremendous interest due to their unique electrical, thermal, and mechanical properties. The effective dispersion of graphene in composite forms a networklike structure, depending on the degree of dispersion, thereby enhancing the electrical and mechanical performance of composites. The presence of percolated structure is necessary for improved electrical conductivity and are extensively reported using plant-derived celluloses, fabricated through chemical-based modifications.[10] The formation of such typical percolative character has boosted practical applications in various fields such as electronics, photonics, biomedical, and sensor applications.[11] The percolation threshold concentrations can be determined using models based on continuum or micromechanics theory,[12] calculated by evaluation of electrical conductivity and structural properties.

To the best of our knowledge, studies considering, *in situ* BC nanocomposite formation with detailed microbial growth kinetics and analysis of percolated structure formation resulting in tunable physicochemical properties of BC/RGO, have not been investigated until now. Many published studies have not considered the effect of carbon-based nanomaterials on fermentation performance and microbial growth behavior which are essential to optimize and predict the scalability of a process. Moreover, the reported studies are more focused on the improvement of physiochemical properties of fabricated nanocomposites to find potential high-performance applications. It should be noted that the presence of such carbon-based nanomaterials (even in trace quantities) as fermentation additives in culture growth media may result in alteration of microbial growth kinetics and bioprocessing behavior, which requires thorough understanding for potential scaled-up operations. Therefore, one of the aims of the current study is to understand the effect of RGO contents on the microbial growth dynamics (under static fermentation), as determined through the bioprocessing kinetic parameters and yield coefficient values. Furthermore, these bionano composites reported in the literature have lowered conductivity and mechanical properties when compared with nanocomposites processed via chemical routes, possibly due to the absence of hierarchal architecture and percolated networklike structures. In present study, the formation of such percolated networks was confirmed from improved mechanical properties and enhanced electrical conductivity, through both experimental and modeling investigations which were scarcely reported in the literature. The proposed *in situ* fermentation technique to produce highly conductive BC/RGO films provides an alternative approach to meet the growing demands of renewable and sustainable biomaterials with commercial significance. Therefore, the current study addressing these challenges is expected to hugely impact in the area of *in situ* bionano composite formation for its novel applications.

The present study reports an *in situ* biosynthesis route for BC/RGO nanocomposites fabrication with improved 2D graphene nanosheets dispersion in nanofiber interlayers. The nanocomposites show the formation of interconnected 3D network confirmed through percolation models which showed an improvement in both electrical and mechanical properties. The microbial growth behavior in terms of kinetics, yield coefficient, and specific growth rate during *in situ* BC/RGO nanocomposite synthesis was studied to get an incite for its commercial process development. The physicochemical properties such as crystallinity, molecular weight, and surface area were investigated to understand the effect of RGO concentrations and fermentation conditions. Molecular mechanism in terms of chemical interactions for the formation of highly integrated networks between BC and RGO was studied in detail. Investigations of structural, thermal, and electrical conductivity properties were carried out to understand the effect of such strong intermolecular hydrogen bonding and presence of percolated-networks on the developed nanocomposites. Therefore, *in situ* BC/RGO nanocomposite synthesis provides a unique approach to fabricate highly flexible and conductive films suitable for novel commercial applications.

■ MATERIALS AND METHOD

Materials. The *Komagataeibacter xylinus* ATCC 11142 used in this study for BC production was procured from Leibniz Institute DSMZ-German Collection of Microorganism and Cell Culture, Germany, in freeze-dried pellet form and further revived as per the protocol. The nutritional components for microbial growth medium were the following: glucose, disodium hydrogen phosphate, citric acid, yeast extract, bacteriological peptone, sodium hydroxide, and calcium carbonate. All the chemicals used in this study were of analytical grade (AR grade) and purchased from Sigma-Aldrich, Finland Oy.

Microorganism and its Revival Process. *Komagataeibacter xylinus* dry pellets were revived as per DSMZ protocol. Revival culture media composed of, glucose (100 g/L), yeast extract (10 g/L), and $CaCO_3$ (20 g/L) with pH adjusted to ~6.8. The inoculated cultures were grown at 37 °C for overnight and subsequently used for further studies. The $CaCO_3$ present in form of the opaque layer was added to neutralize the acids produced during the growth of the microbial strain.

Fabrication and Modification of the Reduced Graphene Oxide (RGO). Graphene nanosheets were produced from the expandable graphite (99.9%, Asbury Carbons (USA)) as detailed in our previous study.[13] The thermal exfoliation under optimized conditions at 750 °C for 2 min in a preheated muffle furnace was used. Partial graphene oxidation was carried out using hydrogen peroxide to improve the dispersion of graphene nanosheets into the fermentation medium. Graphene nanosheets (500 mg), dispersed in methanol was oxidized with the addition of hydrogen peroxide (~2 wt %) through sonication at an amplitude of 30% for 30 min. Excess chemicals were removed by using repetitive centrifugation and washing, followed by drying, to obtain the powdered RGO.

Culture Conditions for the Production of BC/RGO Composites. *K. xylinus* was inoculated (10% v/v) in sterile Hestrin−Schramm (HS) media (g/L): glucose (20.0), yeast extract (5.0), peptone (5.0), disodium hydrogen phosphate (2.5), and citric acid monohydrate (1.15) at pH 6.5, 30 ± 1 °C, and 100 ± 2 rpm for 24 h. The optical density at 600 nm (OD_{600}) was measured (using UV−vis spectrophotometer, PerkinElmer, Lambda 35) and kept constant for each study batch. RGO was added at different concentrations in HS media to form *in situ* BC/RGO composites.

Production Process and Kinetics Study of BC/RGO Nanocomposite Formation. BC fermentation was carried out in 250 mL culture broth inoculated with preculture media, under static conditions at 30 °C for 15 days. The partially oxidized RGO was added to HS medium to achieve suspensions of 1, 2, 3, 4, and 5 wt % followed by autoclaving. The samples (replicative flasks of 20 mL) were collected after time intervals of 1, 3, 5, 6, 7, 9, 10, 11, 12, and 15 days to analyze the microbial growth as well as BC production yield. Control experiment was performed simultaneously without addition of RGO during BC fermentation. All the experiments were performed at least in triplicate, and results mentioned are average ± standard deviation.

Purification and Quantification of BC/RGO Nanocomposite Films. The produced BC membranes were separated (simple filtration) from the fermentation media and squeezed to remove the excess liquid present in it. The cells attached to the BC/RGO nanocomposite membrane were removed by treatment with 0.1 M sodium hydroxide at 80 °C for 90 min. The purified membranes were washed with distilled water for several times until it reaches the pH of ~7 followed by drying at 40 °C in a dry air oven for 3−4 days. The amount of the BC/RGO films produced during each fermentation stages were quantified by measuring the mass over a precision balance. The BC/RGO films thus produced were stored in a desiccator for further studies.

Determination of the Bacterial Cellulose Yield, Cell, and Glucose Concentration. The dry weight (40 °C until constant weight) of *in situ* produced BC/RGO was measured to determine its yield with respect to substrate consumption. The culture media was filtered through a 0.2 μm filter to analyze the unutilized glucose concentration by using high-performance liquid chromatography (HPLC). The HPLC (Waters e2695) was equipped with a differential refractometer detector and autosampler (sample injection volume of 20 μL). An Agilent Hi-Plex H column operated at 65 °C was eluted with 5 mM of sulfuric acid at a flow rate of 0.6 mL/min and calibrated with standard reducing sugar solutions (of cellobiose, glucose, and xylose). The cell biomass was measured by using optical density at 600 nm (OD_{600}). Some cells were possibly trapped inside BC fibers, and hence, they were hydrolyzed by using cellulase (at 50 °C for 1 h) followed by filtration and weighing, as reported by Reiniati et al.[14]

Microbial Growth Kinetics. The Monod equation has been used extensively to determine the microbial growth kinetics[15] and was employed in this study. The exponential or logistic model derived from Monod's equation was used to predict the effect of growth-limiting substrate (S) on the specific growth rate of cells (μ)

$$\mu = \frac{\mu_{\max} S}{K_S + S}$$

where, $\mu_{\max}$ and K_S represent the maximum specific growth rate and Monod saturation constant, respectively. The effect of specific growth rate of microbes, in the presence of different RGO concentrations (from 1 to 5 wt %), was studied by keeping other factors such as pH, temperature, and initial substrate or cell concentrations constant. To better understand the growth kinetic analysis, three different yield coefficients, *viz*, cell growth yield ($Y_{X/S}$), BC yield with respect to cell concentration ($Y_{P/X}$), and substrate consumption ($Y_{P/S}$), were calculated from the following equations:

$$Y_{X/S} = \frac{dX}{dS} = \frac{\text{concentration of cells produced}}{\text{concetration of subsrtate consumed}}$$

$$Y_{P/X} = \frac{dP}{dX} = \frac{\text{concentration of BC produced}}{\text{concetration of cells produced}}$$

$$Y_{P/S} = \frac{dP}{dS} = \frac{\text{concentration of BC produced}}{\text{concetration of substrate consumed}}$$

The kinetic parameters such as specific product formation rate (Q_P) and substrate consumption rate (Q_S) (g/L h) for *in situ* BC/RGO fermentation process were determined using the following equations:

$$Q_P = \frac{1}{X} \times \frac{dP}{dt}$$

$$Q_S = \frac{1}{X} \times \frac{dS}{dt}$$

where X, S, and P are the concentration of cells, substrate, and product of BC/RGO membranes formed (g/L) respectively, during the fermentation process in time (days).

Analytical Methods and Characterization Techniques for BC/RGO Composites. *Scanning Electron Microscope (SEM).* The morphological investigations of produced BC/RGO nanocomposites were carried out by using field emission scanning electron microscopy (FESEM), Zeiss Sigma VP, at an accelerating voltage of 3 kV. Small pieces of films were cut and placed on a stub containing double-sided carbon tape followed by coating with gold for 120 s in a sputtering unit (Emitech K100X). The micrographs were captured and morphological dimensions of the fibers were measured with ImageJ software, averaged over 50 different locations on three different micrographs.

Transmission Electron Microscopy (TEM). The morphological dimensions of the functionalized RGO was investigated using a JEOL JEM 2100 TEM, by drop-casting the RGO suspension (in water) on a carbon-coated copper grid followed by capturing of images at an accelerating voltage of 200 kV.

Fourier Transform Infrared Spectroscopy (FTIR). Physicochemical characterization of the BC/RGO film was carried out with Fourier transform infrared (FTIR) spectroscopy (PerkinElmer, Frontier) by placing thin films onto ZnSe crystals and capturing the spectra in transmission mode. The films were scanned with attenuated total reflection (ATR) accessory in the wavenumber range of 4000−500 cm^{-1} at a resolution of 4 cm^{-1} for 128 scans to obtain the FTIR spectra.

X-ray Diffraction (XRD). The crystal structure properties of BC/RGO films were recorded with X-ray diffractometer (XRD), Rigaku Model SmartLab 4800 equipped with HyPix-3000 2D detector and X-ray source of Cu Kα radiation of wavelength, $\lambda = 1.54$ operating at a voltage of 40 kV and filament emission of 40 mA. The films were

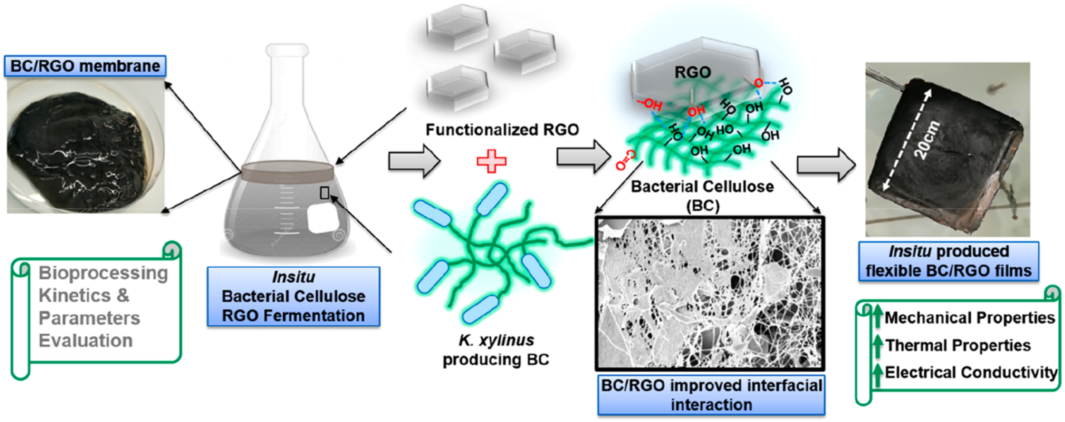

Figure 1. Schematic route of *in situ* fermentation of BC and RGO nanosheets producing films with improved dispersion of graphene due to presence of interfacial molecular forces. (inset) Black-colored BC/RGO pellicles formed at the air−liquid interface directly after fermentation and the air-dried flexible films produced at larger dimensions (20 cm).

placed on a flat sample holder and scanned from a range of 1 to 40° at a step size of 0.01° and a scan speed of 1°/min. The crystallinity index (CI) for the produced BC and BC/RGO nanocomposites were determined using the Segal equation as described below

$$\mathrm{CI} = \frac{I_{002} - I_{\mathrm{am}}}{I_{002}} \times 100$$

where I_{002} represents the intensity of the peak at $2\theta \sim 22.6°$ (002) and I_{am} represents the intensity of the peak of amorphous domains measured from baseline at $2\theta \sim 18°$.

Molecular Weight Distribution (MWD) Analysis. The detailed molecular weight (M_w) characteristics and its distribution were determined using gel permeation chromatography (GPC). For GPC analysis, BC/RGO nanocomposites after fermentation and purification were freeze-dried followed by drying overnight in a hot air oven to remove any trace moisture contents. The samples were initially activated through sequential addition of acetone and *N*,*N*-dimethylacetamide (DMAc) at 45 °C for 4 h followed by dissolving in DMAc/lithium chloride (LiCl) solution, as reported by Shen et al.[16] The samples were dissolved in 90 g/L lithium chloride (LiCl) containing DMAc by vigorous magnetic stirring for 3 days and then diluted to a final concentration of 9 g/L LiCl/DMAc followed by filtration using 0.2 μm syringe filters and finally capped into GPC vials. The samples were analyzed in HPLC, Dionex Ultimate 300 (Sunnyvale CA, USA), fitted with a refractive index detector, Shodex RI-101 (Tokyo, Japan). The HPLC was connected with a guard column and four analytical columns (PLgel Mixed-A, 7.5 × 300 mm) in which a flow rate of 0.75 mL/min and temperature of 25 °C was maintained for the eluent. The HPLC was precalibrated using narrow pullulan standards (343 Da−2500 kDa; PSS, Mainz, Germany) and M_w corresponding to cellulose was calculated as per earlier reported literature.[17]

X-ray Photoelectron Spectroscopy (XPS). The surface chemical characteristics of the BC and BC/RGO films were analyzed with XPS spectroscopy (AXIS Ultra spectrometer), utilizing a monochromatic Al Kα radiation at 100 W and data analyzed and fitted using CasaXPS software for carbon (C) and oxygen (O) content. Samples were evacuated in vacuum for overnight followed by a survey and high-resolution scans of C 1s and O 1s over an area of 1 mm^2 recorded on 2−3 different locations, with scan depth of <10 nm.

Raman Spectroscopy. BC/RGO films were scanned with WITec alpha300 R Raman microscope (alpha 300, WITec, Ulm, Germany) using an Nd:YAG green laser with an excitation wavelength of 532 nm measured with an exposure time of 5 and 1024 scans.

Surface Area Analysis (SA). For surface analysis measurements, the BC/RGO membranes after fermentation and purification were frozen by immersing them in liquid nitrogen maintained at −196 °C. Thereafter, the frozen membranes were freeze-dried using Labconco FreeZone 2.5 Freeze-Dryer operating at −53 °C and 0.113 mbar for 24 h. Nitrogen physiosorption measurements were carried out at 77 K and various relative pressures using a gas adsorption analyzer (Micrometrics, TriStar II 3020) to measure the Brunauer−Emmett−Teller (BET) surface area.

Dynamic Mechanical Analyzer (DMA). The mechanical properties of produced BC/RGO films were measured using a DMA, TA Instruments, DMA Q 800. The BC/RGO films were cut into dimensions of 3 cm × 1 cm (length × width) and thickness was measured using a digital micrometer thickness gauge (Dicfeos). The measurements were carried out with clamp film tension geometry at room temperature equipped with a 20 N load cell at a constant speed of 1 mm/min.

Thermogravimetric Analysis (TGA). The thermal properties of BC/RGO nanocomposite films were measured with a TGA, TA Instruments, Q 500 (New Castle, DE, USA) equipped with a platinum crucible under inert conditions. BC/RGO films (of weight ∼3−4 mg) were heated from room temperature to 600 °C at a heating rate of 10 °C/min in the presence of nitrogen gas flow (of ∼30 mL/min) and change in thermogravimetric signals and its derivative (DTG) was recorded.

Electrical Conductivity. BC/RGO films of dimensions (1 cm (length) × 1 cm (width)) were connected to four points linear probe (Jandel Model RM3000 test unit, Jandel Engineering Ltd.) to measure the sheet resistance using a Keithley 2400 as source meter. The thickness of the films was measured with a digital micrometer thickness gauge to determine the electrical conductivity (S/cm).

■ RESULTS AND DISCUSSION

***In Situ* BC/RGO Synthesis by Using *K. xylinus*.** Figure 1 shows the overall *in situ* BC/RGO film formation approach by using *K. xylinus* and functionalized graphene under static aerobic conditions. The RGO flakes were produced and subsequently functionalized to induce hydroxyl and epoxy groups in its backbone which resulted in their improved dispersion and prolonged stability in culture media. The RGO addition in culture media was considered to be homogeneous even at higher concentrations (1−5 wt %) which is confirmed by the consistent black media color (further confirmed through XPS and FTIR studies in subsequent sections). This is probably because the culture media is a complex mixture of polysaccharides, proteins, peptides, amino acids, etc., which acts as an enhanced dispersion agent and reducing agent, as discussed in subsequent sections. Earlier reported studies have shown that RGO dispersed in water forms a stable suspension, without any significant aggregations for almost 3 weeks, which

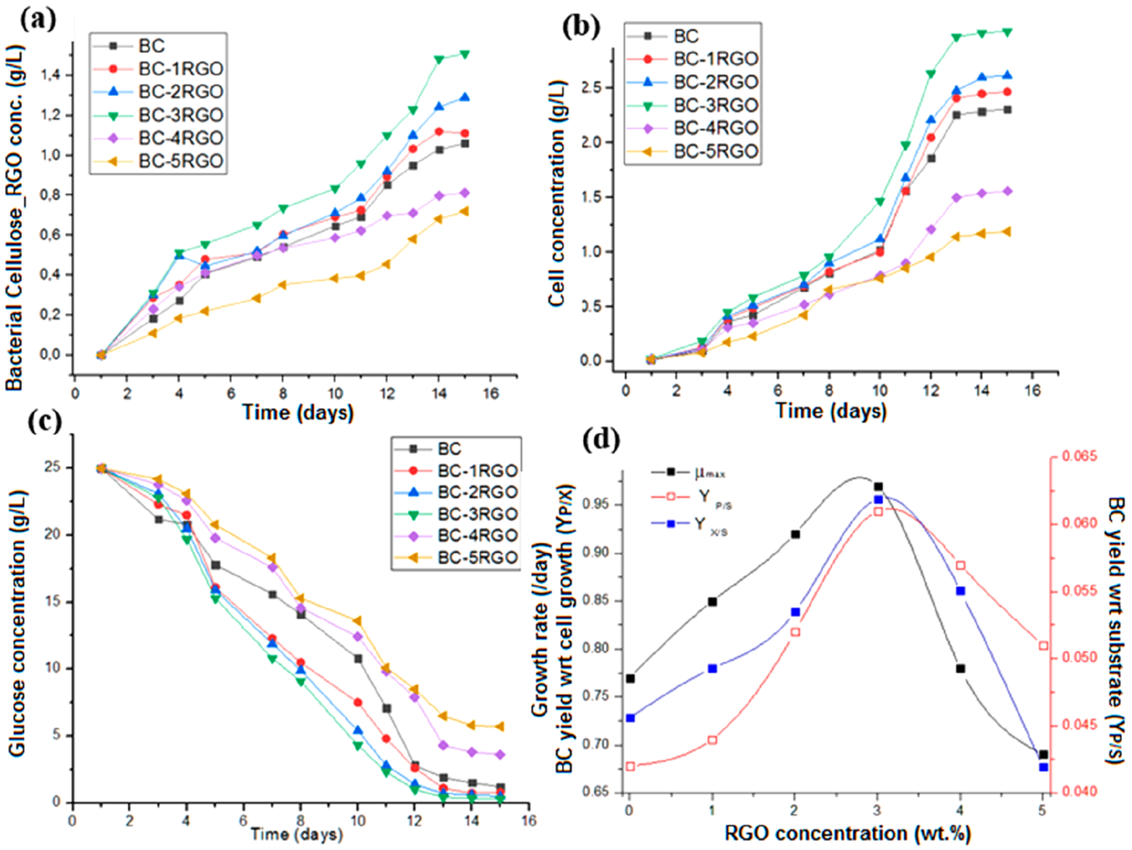

Figure 2. Effect of RGO concentration on *K. xylinus* ATCC 11142 cultivation performance under static conditions at pH 6.5 and 30 °C. (a) Production of bacterial cellulose (measured in grams per liter), (b) biomass concentration (g/L), (c) glucose consumption, and (d) change in kinetic parameters, i.e. maximum specific growth rate (μ_{max}) and yield coefficients $Y_{P/X}$ and $Y_{P/S}$.

falls within the time regime of BC fermentation carried out for ~15 days.[18] The culture media gradually changed its color from a blackish to yellowish suspension with the intercalated RGO in between growing BC fibers (initiating from ~3 days of fermentation), suggesting improved interfacial interaction and adhesion between two systems. Due to the presence of such improved hydrogen bonding based interactions (as discussed in subsequent section), it was assumed that major fractions of RGO were incorporate in the intergalleries of BC nanofibers, in line with the earlier reported studies.[9] Furthermore, it was observed that a three-dimensional BC/RGO hydrogel containing a physically cross-linked network of BC nanofibers with dispersed RGO sheets in between was produced at the air−water interface. Moreover, it was also observed that the partially oxidized RGO underwent gradual reduction. This has a significant effect in enhancing the electrical conductivity of films along with improved mechanical and thermal properties which could be used for producing free-standing flexible BC/RGO films (Figure 1). The reducing effect of culture media on the growth kinetics of BC and their subsequent effect on the physio-chemical and structural properties of fabricated BC/RGO nanocomposite films have been studied and discussed in subsequent sections.

Microbial Cell Growth Kinetics Study during *in Situ* BC/RGO Nanocomposite Formation. Production of BC is significantly affected by the type of bacterial culture, reactor system, pH type of carbon source used, temperature, and oxygen limitation conditions.[19] However, reports studying the effect of nanofiller (such as RGO) incorporation on microbial dynamics and BC production have seldom been reported. The inoculated growth medium was completely found to be black initially due to the presence of dispersed RGO, with no significant presence of BC pellicles. The culture during this period showed lag phase, adapting to the changing environmental conditions (Figure 2a and b), which was prevalent in all concentrations of RGO used. However, microorganisms enter in exponential phase after 3 days that eventually starts the formation of BC pellets at the air−media interface with clear media color changes. The metabolic activities in exponential phase are rapid and thus increased glucose uptake rate was observed after 3 days.

The rate of biomass formation and substrate utilization shows variation with different RGO concentrations (Figure 2c and d). The 3 wt % RGO shows the highest maximum specific growth rate (μ_{max}) of 0.122 1/day. This is possibly because *K. xylinus* are Gram-negative bacteria rich in phospholipids or lipopolysaccharides on their cell membranes[20] which provides improved hydrophobic interactions with RGO. Further increase in RGO content in BC fermentation medium from 4 to 5 wt %, resulted in decreased μ_{max} values to 0.062 and 0.049, respectively, suggesting an inhibitory effect of RGO on cell growth at higher concentrations. The biomass concentrations were increased with the rapid uptake of glucose until 12 days of fermentation (Figure 2). It was observed that due to substrate limitations of glucose in the medium (Figure 2 c) as well as oxygen limitation due to BC layer formation at air-media interface, resulted in a deceleration of cell growth rate with constant BC yield. The glucose remained in the medium

DOI: 10.1021/acsabm.9b00581
ACS Appl. Bio Mater. 2019, 2, 4052−4066

Table 1. Kinetic Process Parameters Determined for *in Situ* Fermentation by Using *K. xylinus* ATCC 11142 under the Static Condition at 30 °C for 14 Days

process parameters	BC	BC-1RGO	BC-2RGO	BC-3RGO	BC-4RGO	BC-5RGO
Bacterial Cellulose Production						
cellulose (g/L)	1.06	1.11	1.29	1.51	0.81	0.72
Q_P (g/L day)	0.03	0.02	0.030	0.039	0.031	0.025
$Y_{P/S}$ (g/g)	0.042	0.044	0.052	0.061	0.057	0.051
$Y_{P/X}$ (g/g)	0.460	0.449	0.492	0.50	0.519	0.605
Substrate Consumption						
glucose consumed (%)	95.2	96.9	98.0	98.8	85.6	77.2
Q_S (g/L day)	0.796	0.773	1.09	1.29	0.755	0.652
Cell Growth Parameters						
$Y_{X/S}$ (g/g)	0.091	0.098	0.106	0.122	0.109	0.084
cell (g/L)	2.31	2.47	2.62	3.02	1.56	1.19
μ_{max} (1/day)	0.77	0.85	0.92	0.97	0.78	0.69
K_S (g/L)	1.2	2.6	5.4	7.2	4.3	5.0

after 12 days was only 1.2−4.8% for 1−3 wt % of RGO in culture suggesting the substrate limitation to the fermentation process. Therefore, *K. xylinus* in the stationary phase (after 12−15 days) are still metabolically active to produce higher BC. This behavior suggests that *K. xylinus* based BC is a mixed growth-associated production. Microorganisms utilize glucose in exponential phase to increase the biomass and then subsequently convert that biomass into BC until the stationary phase. The extent of the stationary phase varies with RGO concentration (Figure 2b). The pH of fermentation media for both the BC and BC/RGO after 15 days was within the range of 4−4.5. HPLC analysis showed that the concentration of gluconic acid (fermentation metabolite) both in case of pure BC and BC/RGO fermentation (after 15 days) did not show any significant difference in the presence of varied RGO concentration. Therefore, it could be inferred that addition of optimized concentrations of RGO (up to 3 wt %) significantly improved the cell growth and BC production, while higher RGO (>4 wt %) suppressed the cell growth and BC production.

Table 1, summarizes the kinetic process parameters, yield coefficients, specific substrate consumption rates, and BC/RGO production under different RGO concentrations after 15 days of fermentation. The BC yield in control media was 1.06 g/L, which gradually increased to 1.51 g/L with the incorporation of 3 wt % RGO. An increased glucose consumption as evident from Q_S values resulted in higher bacterial metabolism forming a thick BC/RGO hydrogels after 15 days of fermentation. Figure 2d shows the effect of RGO content on yield coefficients for BC/RGO nanocomposite formation with respect to the substrate, cell concentration, and maximum specific growth rate. The kinetic parameters and yield coefficients have a parabolic effect with increasing RGO content, reaching maxima at 3 wt % RGO, suggesting it to be an optimal concentration favoring the microbial growth as well as *in situ* nanocomposite formation. It was also observed that increased RGO concentration (up to 5 wt %) shows a detrimental effect on microorganisms that resulted in lowered μ_{max} values. It was observed that RGO due to its favorable interaction acts as a support to BC formation, which changes the metabolism rate for BC formation but due to its inert nature is unlikely to alter the BC metabolic pathway. From the kinetic study, it was concluded that the presence of RGO tunes the microbial growth dynamics as well as the production of BC fibers during the *in situ* fermentation process. The BC/RGO films thus formed are expected to show improved physicochemical and structural properties which are evaluated and discussed in subsequent sections.

Effect of Fermentation Conditions and RGO Concentration on Physicochemical Properties of BC/RGO Nanocomposite. The physicochemical properties of BC/RGO nanocomposites are expected to alter with varied RGO concentrations in the fermentation medium. Figure 3a, explains XRD diffractograms of BC/RGO films showing the peaks at 2θ = 14.8°, 16.5°, and 22.6° corresponding to cellulose I crystal planes of BC at $(1\bar{1}0)$, (110), and (200), respectively, and at 2θ = 26.5° (002) representing the RGO crystal lattice. The crystallinity indices (CIs) of BC/RGO decreased gradually from 75.1% (for pure BC) to 63.1% with the addition of RGO (up to 5 wt %). Interestingly, this decrease in CI in the presence of RGO (although productivity was increased up to 3 wt %) can be ascribed due to the improved interaction between BC and RGO nanoflakes. The presence of hydrogen-bonded interactions provide hindrance for effective packing of BC chain into highly crystalline segments.[21] Moreover, it is well-known that the high M_w and DP_w of BC chains will require higher energy to fold into crystalline structures. The presence of RGO results in hindrance toward effective BC chain packing into highly crystalline structures during its biosynthesis process (especially at 3 wt % RGO), resulting in reduced crystallinity indices values. Furthermore, the presence of RGO diffractogram peak in all nanocomposites suggests uniformly dispersed RGO nanosheets intercalated within BC matrix.

The surface behavior of BC and BC/RGO nanocomposites were evaluated by using FTIR spectrographs (Figure 3b). BC shows characteristic FTIR peaks at 3345, 2884, 1636, 1422, and 1057 cm^{-1} corresponding to the hydroxyl (−OH) stretching vibrations, −CH asymmetric stretching (corresponding to CH_2 and CH_3 groups), hydroxyl (−OH) bending vibrations, CH_2 symmetric bending, and C−O skeletal stretching, respectively.[22] The FTIR spectrograph of functionalized RGO sheets shows the presence of peaks at 3550 cm^{-1} representing O−H stretching; 1200 cm^{-1} corresponding C−O epoxy stretching; 1070 and 1720 cm^{-1} denoting the C−O alkoxy and C═O carbonyl stretching vibrations, respectively, suggesting the presence of hydroxyl and epoxy groups in its backbone. With the introduction of RGO; significant alteration in the intensity of peaks at 3345 cm^{-1} and appearance of a new peak at 1570 cm^{-1} was observed with increased peak intensity.

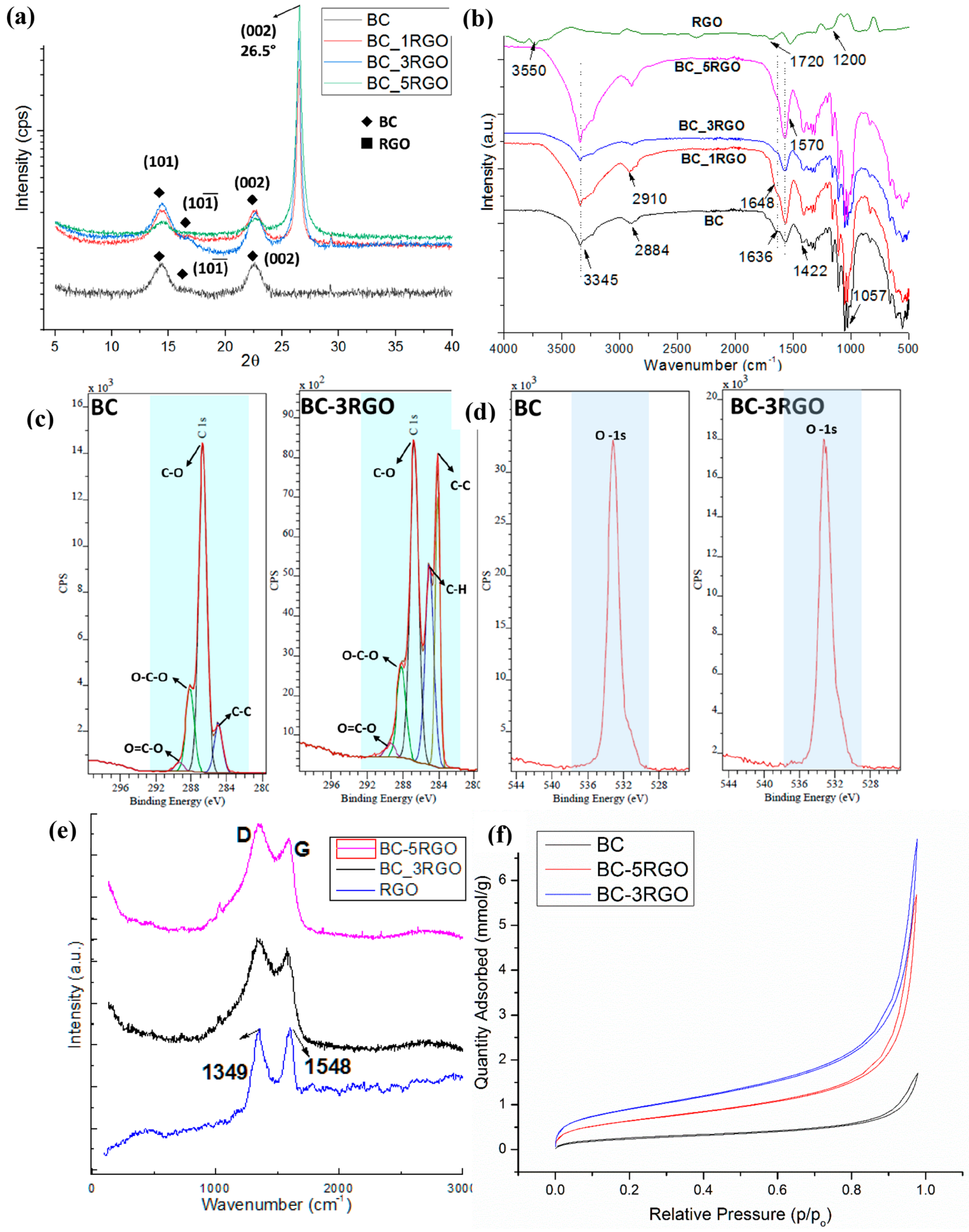

Figure 3. Characterization of different BC/RGO composites produced by using *K. xylinus* ATCC 11142 at various RGO loadings. (a) XRD pattern, (b) FTIR spectroscopy, high resolution (c) C 1s XPS spectra, (d) O 1s XPS spectra, (e) Raman spectroscopy, and (f) nitrogen adsorption/desorption curve.

The peak at 3345 cm^{-1} represents the stretching vibrations of BC hydroxyl group, which shows reduced intensity with increased RGO content up to 3 wt %. Similarly, the peak at 1570 cm^{-1} represents the antisymmetric stretching vibrations of carboxylate groups that show a gradual increase in peak intensity with RGO addition. This is possibly because of strong hydrogen-bond interactions between partially oxidized RGO and BCs as well as gradual reduction of RGO during *in situ*

Table 2. Evaluation of Physicochemical Properties of *in Situ* BC/RGO Films Produced by Using Fermentation at Different RGO Loadings

process parameters	BC	BC-1RGO	BC-2RGO	BC-3RGO	BC-4RGO	BC-5RGO
Crystal Properties						
crystallinity index (CI)	75.1	70.3	67.6	67.8	65.0	63.1
Surface Area Properties						
BET surface area (m^2/g)	20.2	43.8	47.5	73.8	54.8	52.5
avg pore size (nm)	9.7	9.5	11.2	14.4	10.4	10.9
total pore volume (cm^3/g)	0.12	0.18	0.32	0.23	0.28	0.21
Physical Properties						
molecular weight (M_w)	420190	439872	490348	512342	504990	419234
degree of polymerization (DP_w)	2335	2440	2725	2845	2805	2330

fermentation process. However, at RGO content >4 wt %, the peak intensity corresponding to −OH vibrations as well as O−C−O stretching was found to be unaltered, suggesting possibly agglomerations of RGO. The XPS study was carried out to confirm the *in situ* reduction of partially oxidized RGO during the fermentation process, as shown in Figure 3c and d. XPS analysis for both BC and BC/RGO shows significant variation in terms of C and O elemental analysis as evident from high-resolution spectra of C 1s and O 1s. The C 1s spectra of BC (Figure 3c) shows four distinct peaks at 284.6, 286.7, 287.5, and 288.5 eV corresponding to C−C, C−O, O−C−O, and O−C═O bondings, respectively. BC/RGO films showed an additional peak at 285.5 eV representing the C−H vibration along with increased intensity of C−C or O−C−O peaks.[23] This indicates the stretching of hydroxyl groups present on BC due to the occurrence of intramolecular hydrogen bonding, which is in agreement with FTIR analysis. However, O 1s spectra of BC/RGO shows reduction in the peak intensity compared to BC (Figure 3d) suggesting possible reduction of partially oxidized RGO during *in situ* fermentation process. This may be due to the presence of the yeast extract in fermentation medium or interaction of RGO with highly reducing hydroxyl groups of BC fibers. A similar observation in reduction of graphene oxide to RGO was observed by Nandgaonkar et al.,[24] explains the reducing tendency is due to yeast extract, present in growth media. It is also expected that simultaneous reduction of RGO as well as hydrogen-bonded interaction, improves the adherence of graphene nanosheets with BC fibers forming an interconnected 3D network during fermentation. Therefore, both FTIR and XPS spectroscopic studies confirm the presence of interfacial interaction between RGO and BC during *in situ* cultivation. This interaction between RGO and BC are expected to tune the physicochemical properties of BC/RGO as discussed in the subsequent sections.

Lastly, Raman spectroscopy of BC/RGO films was also studied to confirm the structural changes and functionalities during biosynthesis. The Raman spectra for RGO nanosheets shows two characteristic peaks at 1349 and 1584 cm^{-1} demonstrating D and G bands, respectively with an $\frac{I_D}{I_G}$ ratio of 0.98 (as shown in Figure 3e). The D band corresponds to defects in carbon backbone, and the G band arises due to the presence of sp^2 hybridization in graphitic layers. The ratio of $\frac{I_D}{I_G}$ provides a tool to measure structural disorders/defects or impurities arising in the carbon materials during processing. With RGO nanosheets introduction to BC fibers during *in situ* fermentation showed a slight increase in $\frac{I_D}{I_G}$ ratio to 1.02 and 1.03 at 3 and 5 wt % of RGO loadings, respectively. The increase in intensity ratio was observed to be very low, suggesting the presence of improved interfacial interaction that resulted in the removal of oxygen moieties from RGO sheets. This also suggests that RGO sheets structurally did not undergo significant changes during *in situ* fermentation. Therefore, high-quality RGO nanosheets without any defects were still present after 15 days of bioprocessing.

The effective dispersion of RGO intercalated within the BC network is expected to form a porous structure which will remain stable under freeze-dried conditions. Therefore, to evaluate the surface area and pore structure characteristics of BC/RGO nanocomposites, the nitrogen gas adsorption−desorption analysis was done at 77 K (Figure 3f). The BET surface area of BC/RGO was three times higher (S_{BET} ∼ 73.8 m^2/g at 3 wt % RGO) than pristine BC (S_{BET} ∼ 20.2 m^2/g). The S_{BET}, average pore size, and pore volume were decreased at higher RGO loadings (>4 wt %). The presence of large pore dimensions and high specific surface area of BC/RGO nanocomposites in comparison to pristine BC confirms that RGO nanosheets show inherent high surface area characteristics. RGO nanosheets could effectively form support that prevents the shrinkages of pores during the freeze-casting process.[9] Furthermore, for all BC and BC/RGO nanocomposites, the characteristic physio-sorption curves follow a type IV isotherm with the presence of a hysteresis loop that extends up to a relative pressure (P/P_o) of 1. However, RGO tends to agglomerate at higher concentrations (>3 wt %) under hydrophilic conditions which were evident from the reduced S_{BET} and average pore size/volume values (52.5 m^2/g at 5 wt % RGO).

The effect of RGO on macromolecular properties of BC/RGO nanocomposites, such as average molecular weight (M_w) and degree of polymerization (DP_w) were investigated, as reported in Table 2. Although, the culture media contained chemically inert RGO nanosheets; it showed physicochemical interactions with the growing bacteria due to the presence of partially oxidized functional groups and hydrophobic surface characteristics. The presence of such interactions have shown to affect the microbial growth kinetics and may alter the metabolic cellulose biosynthesis capability of *K. xylinus*. The produced BC fibers have characteristic M_w and DP_w of ∼420 kDa and ∼2335 respectively, which is in line with the earlier reported studies.[25] Interestingly, BC/RGO (up to 3 wt % RGO), was found to increase both M_w and DP_w considerably up to 22% during *in situ* fermentation. This increase may be evident due to the improved specific growth rates and yield coefficients which eventually accelerates BC biosynthesis flux. Additionally, the RGO present in culture media interacts

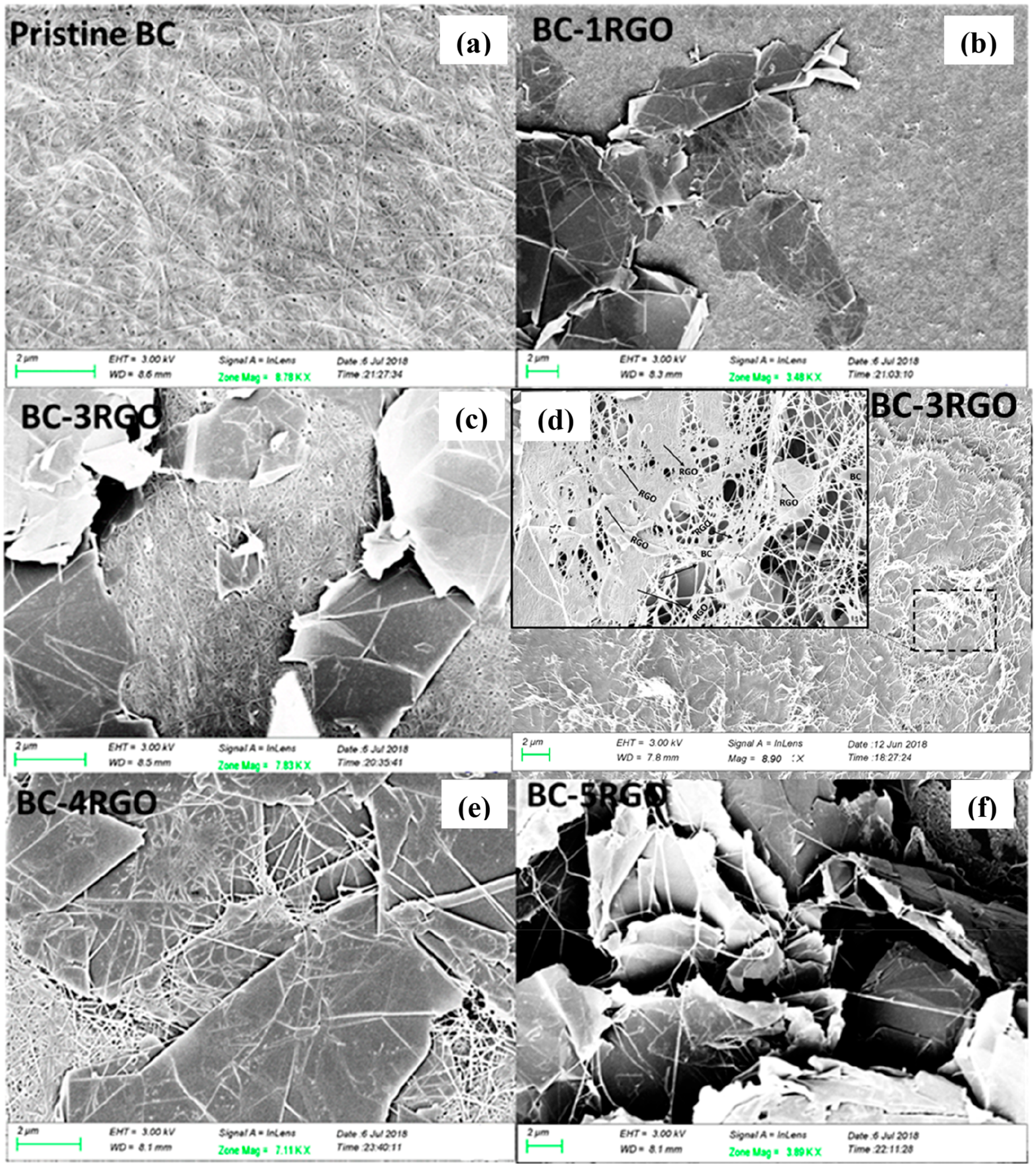

Figure 4. FESEM micrographs of BC/RGO films produced through *in situ* fermentation. Surface morphology of (a) pure BC films, (b) BC-1RGO, and (c) BC-3RGO nanocomposite, (d) cross-sectional view of BC-3RGO film, (e) surface morphology of BC-4RGO, and (f) surface morphology of BC-5RGO films.

(hydrophobic) with cell membrane of Gram-positive *K. xylinus*. The presence of such interactions during *in situ* fermentation makes RGO as unique support and helps in the proliferation of *K. xylinus* for growth as well as BC formation with improved yields. However, higher RGO loadings show a detrimental effect on both microbial growth kinetics as well as M_w and DP_w distribution. Therefore, present investigation shows that physicochemical properties of BC/RGO films can be uniquely controlled by the state and kinetics of *in situ* fermentation, which provides an alternative, and novel approach to tailor the nanocomposite characteristics.

Morphological Characterization of BC/RGO Composites. Field emission SEM microscopic analysis was carried out to investigate the surface morphology and degree of *in situ* hybridization between RGO nanosheets and BC nanofibers formed during fermentation. The pristine BC films show translucent and whitish color with highly entangled and continuous layers of fibers of diameter ~55 ± 8 nm (Figure 4a). The functionalized RGO nanosheets have a lateral dimension of ~3.8 ± 0.8 µm (as shown in Figure S1 in the Supporting Information). It was observed that the incorporation of RGO during *in situ* BC biosynthesis resulted in three different types of morphologies depending on concentrations used. First, at lower concentrations of added RGO (1−2 wt % RGO), the graphene nanosheets were found to be segregated from each other forming isolated patches in the mesh of BC fibers (Figure 4b). The dimension of BC fibers produced was found to be almost unchanged for 1−2 wt % RGO (diameter

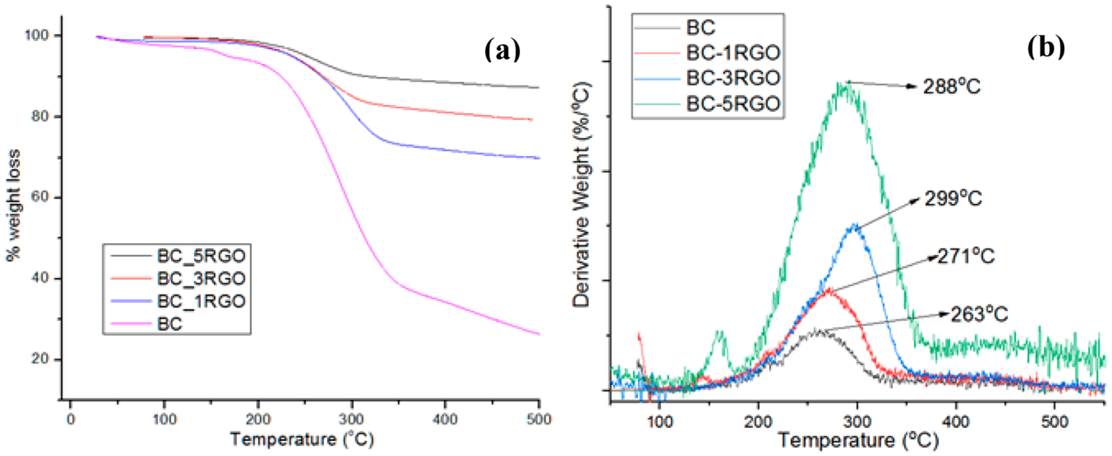

Figure 5. Thermal property evaluation of BC/RGO nanocomposites produced with different RGO loadings. (a) TGA profile and (b) DTG thermographs produced through *in situ* fermentation.

48 ± 9 and 40 ± 11 nm, respectively). With increasing RGO concentrations (up to 3 wt %), graphene nanosheets were uniformly dispersed in interlayers of BC fibers (Figure 4d) with improved interfacial adhesion resulting in the formation of a smooth interface between two discrete nanomaterials. From the high-resolution FESEM micrograph (inset of Figure 4d), it was observed that the RGO sheets are intercalated in between the BC fibers forming a physical entanglement resulting in nested or networklike structure. The presence of a smooth interface between the two discrete nanomaterials suggests improved interaction or interfacial adhesion arising from the intermolecular hydrogen-bonding as well as gradual reduction of RGO (discussed in earlier section) during *in situ* fermentation approach. The fiber morphology was also found to be similar in nature, with a slightly lowered diameter of 32 ± 9 nm. The lowered fiber diameter increases the aspect ratio and is expected to act as better reinforcing agents (Figure 4 c). BC fibers were found to be effectively growing, overlapping and wrapping up on the surface of RGO sheets possibly due to enhanced compatibility arising from intramolecular hydrogen bonding and hydrophobic interactions. It was also observed that during *in situ* fermentation process the initial layer of thin BC/RGO hydrogel forms at the air−liquid interface which gradually thickens with cultivation time through a layer-by-layer approach. This layer-by-layer formation of BC/RGO films supports graphene sheets to undergo the formation of 3D structures with interconnects between neighboring RGO sheets to establish a percolated network-like structure. The cross-sectional view of BC-3RGO film (Figure 4d) confirms the presence of layered structures including BC fibers in alternate galleries of RGO nanosheets, creating a dense physical entanglement, which acts as interweave for linking them. The presence of similar hierarchal architecture was observed in artificial nacres made up of self-assembled nanocellulose and graphene processed through chemical approaches.[26−28] The formation of such network through biochemical fermentation process results in the creation of a conductive pathway as well as reinforcing systems, which was confirmed through electrical conductivity and mechanical property assessment as discussed in succeeding sections. Third, at higher RGO concentrations (4 or 5 wt %) agglomerate (diameter ∼ 55 ± 10 and 58 ± 5.5 nm, respectively) of RGO sheets were found which resulted in formation granular surface and nonuniform morphology. Although BC-4RGO film was uniform, BC-5RGO film showed the presence of pores or voids suggesting the incompatibility between them. Therefore, morphological investigations showed that dispersion of RGO sheets in BC matrix exists in three different forms (shown schematically in Figure 7), which is expected to govern the overall structural and electrical conductivity properties of nanocomposites, as discussed in successive section.

Thermal Properties of the BC/RGO Composites. Thermal behavior of BC/RGO nanocomposites was evaluated to determine the effect of RGO on the onset and peak degradation temperatures (T_{onset} and T_{p}) and residual fraction of ash content (%). It is evident from the earlier discussion that integration of BC nanofibers into RGO sheets is expected to significantly alter the thermal properties of the nanocomposites. However, previous studies on *in situ* biopreparation of BC/GO have shown a significant drop in thermal properties of prepared nanocomposites, probably due to poor dispersion or incompatibility of GO with the BC matrix resulting in phase separation.[29] The present approach for *in situ* fermentation of BC/RGO shows that incorporation of RGO significantly improved the thermal properties of fabricated nanocomposite films, which was prevalent in all RGO concentrations used. The pristine BC films showed a drop in weight by ∼5% when heated up to 200 °C due to the removal of trapped moisture with T_{onset} of 205 °C and T_{p} of 263 °C, respectively (Figure 5a). The thermogravimetric analysis (TGA) profile of *in situ* produced nanocomposites showed a single step degradation profile which was also confirmed from the derivative of thermograms (DTG) (with a single maxima peak) that remained unaltered even at higher fractions of RGO added (Figure 5b). The BC/RGO films at all RGO concentrations showed three main degradation profiles: (i) removal of absorbed moisture from films due to hydrophilic nature of BCs which decreases with increase in RGO concentration, (ii) onset and peak degradation steps which are due to depolymerization of BCs through cleavage of glycosidic bonds,[30] and (iii) at temperatures above 400 °C, release of gaseous products such as carbon dioxide or carbon monoxide and presence of unconverted byproducts as solid ash content. From DTG plots, it was observed that T_{p} increased to 271, 288, and 299 °C with the addition of RGO at 1, 3, and 5 wt % respectively, via the *in situ* fermentation approach (Figure 5b). Furthermore, from residual ash content analysis, it could

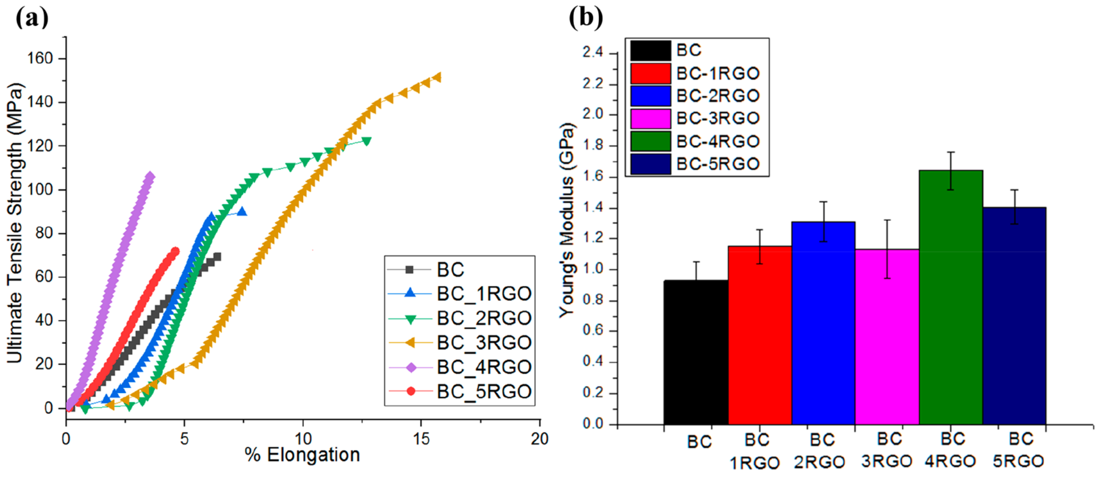

Figure 6. Mechanical property assessment of BC/RGO nanocomposites produced at different RGO loadings. (a) Tensile stress−strain plot and (b) Young's modulus of for the*in situ* produced BC/RGO nanocomposite.

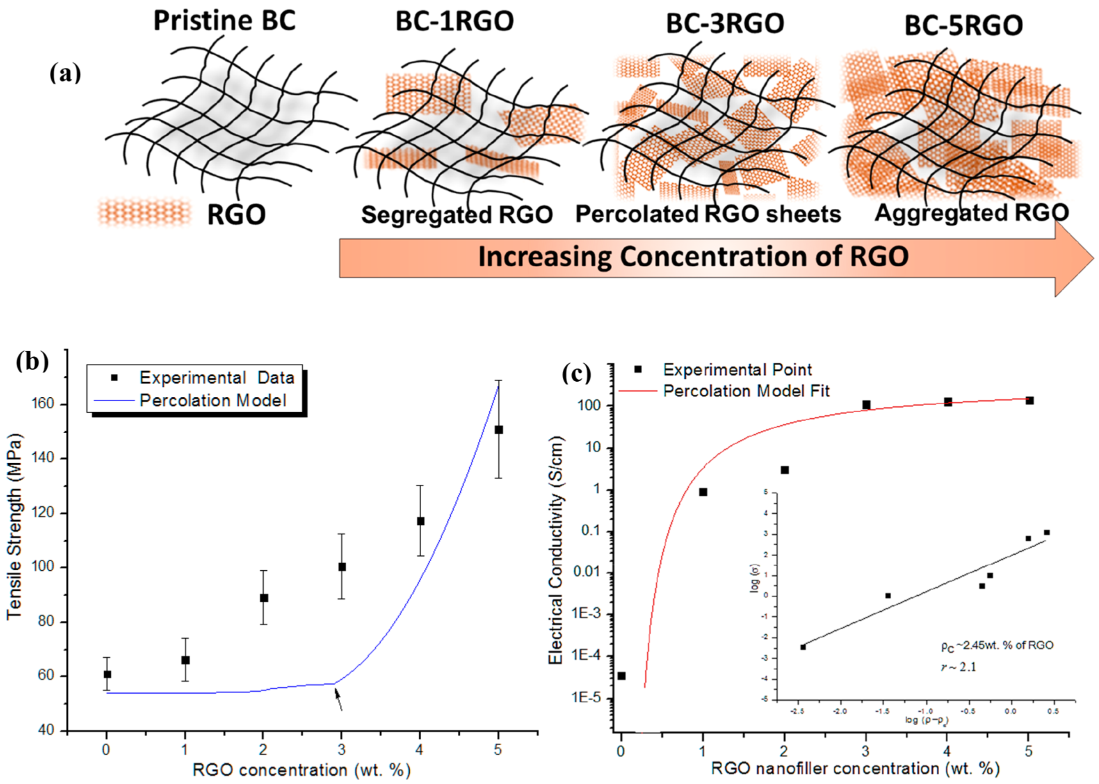

Figure 7. (a) Schematic representation of percolated-network formation with increased RGO concentration during *in situ* BC/RGO composite fermentation process, (b) mechanical properties of BC/RGO nanocomposite films fitted with the classical mechanical percolation model, and (c) electrical conductivity values fitted with the power scaling law, for the BC/RGO nanocomposite films produced different RGO loadings. (inset) Linear fit of the log−log plot of conductivity versus ($\rho - \rho_c$) with the calculated universal critical exponent, $r \sim 2.1$ wt % of RGO.

be confirmed that RGO addition lowered the BC fiber conversion to gaseous products at temperature above 400 °C, due to their increased thermal stability. The residual ash content was increased from 25% for pure BC fibers to 75%, 81%, and 86% with the increased addition of RGO (1, 3, and 5 wt %, respectively). The improved thermal stability is due to efficient interfacial interactions of RGO and BC fibers using physical forces such as hydrogen bonding or hydrophobic interactions arising during *in situ* reduction of RGO. Inherently, graphene has high thermal conductivity[31] and as it effectively wraps or integrates with the BC fibers (evident from morphological analysis) during the *in situ* fermentation process it eventually resulted in their enhanced thermal stability. Therefore, the proposed route of *in situ* BC/RGO nanocomposite fabrication provides an alternative and sustainable approach with enhanced thermal stability highly comparable with chemical-based modifications.[32]

Mechanical Behavior of *in Situ* Fabricated BC/RGO. The mechanical behavior of BC/RGO films produced via *in situ* fermentation process was investigated from stress−strain curves to determine the reinforcing capabilities of RGO platelets. The ultimate tensile strength (UTS) was found from the typical stress−strain curve of BC film was 65 MPa with an elongation at break of 7%, which are similar to earlier reported literature.[33] However, it has been reported that UTS largely depends on the cultured microorganism, carbon/nitrogen source in media, and other fermentation operational conditions.[34] BC-3RGO films showed almost two times increase in tensile strength of 151 MPa, as compared to pristine BC films. Simultaneously, the percentage elongation at break of BC-3RGO was almost doubled and enhanced up to 16%. An improvement in both tensile modulus and elongation at lower loadings of RGO, suggests the formation of nanocomposites with higher toughness and stiffness. Moreover, as confirmed from spectroscopic studies, the presence of intermolecular hydrogen bonding and hydrophobic interactions between BC and RGO platelets, are responsible for improved mechanical behavior. The earlier reported studies on *in situ* BC/RGO films production through chemical or fermentation routes have shown improvement in tensile modulus with reduced strain or percentage elongation.[9] The current study's evaluation of Young's modulus (YM) for BC/RGO nanocomposites showed improvement as compared control BC films that remained within the range of 1.2−1.6 GPa, suggesting the highly flexible nature of films (Figure 6).

The added advantage of using *in situ* BC/RGO production by the fermentation strategy is the formation of a percolated network and hierarchical organization of BC in the interlayers of RGO, resulting in the formation of high strength and elastic films.[35] The formation of a layered structure in BC/RGO films was confirmed from morphological investigations (Figure 4d). However, the presence of a percolatedlike structure was predicted through the Ouali model.[36] It has been observed that the presence of strong matrix−filler interaction is induced through electrostatic interactions or hydrogen bonding, which results in the formation and growth of the network. The theoretical volume fraction (ϕ_c) can be calculated from percolation theory[37] as

$$E_c = \frac{(1 - 2\phi\psi)E_mE_f + (1 - \phi)\psi E_f^2}{(1 - \phi)E_f + (\psi - \phi)E_m}$$

$$\psi = 0 \quad \phi \leq \phi_c$$

$$\psi = \left(\frac{\phi - \phi_c}{1 - \phi_c}\right)^b \quad \phi > \phi_c$$

where the ϕ is the volume fraction of RGO, E_m, E_f, and E_c are shear moduli of BC, RGO, and the prepared BC/RGO nanocomposite, respectively, b is critical exponent, and ψ is the volume fraction of the percolating filler network. BCs are made up of high aspect ratio nanofibers, without any detectable chain ends. Therefore, it is assumed that the BC backbone is responsible for effective stress transmission when dispersed in the nanocomposites.[38,39] Hence, as per De Gennes et al.,[40] the critical exponent is assumed to be 1.8. In present study, from the mechanical percolation model, the critical percolating threshold concentration was found to be 3 wt % of RGO (Figure 7b). From the experimental studies, it was observed that no appreciable improvement in stiffness was observed at lower RGO loadings of 1 wt %. However, the mechanical behavior improved with higher RGO loading of 3 wt % following the trend as predicted by the classical percolation theory.[37] This suggests that the percolation network formation was initiated in the presence of 2 wt % RGO which extensively grows following the percolation scaling law. During percolation formation, two main macroscopic phenomena undergoes. First, the formation of entanglements of BC fibers with RGO platelets which grows into a rigid nanofibrillated network and second, with increased interfacial contacts between dispersed RGO and BC fiber at nanoscale dimensions (as shown in Figure 7a). The degree of reinforcement by such networks is governed by molecular forces such as hydrogen bonding arising from high hydroxyl functionality of BC fibers and *in situ* reduction of RGO sheets during the fermentation process. This leads to strong contact strength between filler and matrix, which resulted in effective transfer of the high elastic modulus of the graphene sheets to the BC fibers. However, higher loadings of RGO nanosheets are known to undergo agglomerations and cause lowered tensile strength as well as strain at break which was evident from the presence of pores and voids in the electron micrographs of BC-5RGO (Figure 4f). Therefore, the present study shows that *in situ* BC/RGO nanocomposite fermentation resulted in high strength films with improved toughness and flexibility. The underlying mechanism for percolation formation needs further investigations. The evaluation and existence of such a percolation network in BC/RGO nanocomposites is also detectable from the electrical conductivity properties, which were assessed in the next section.

Electrical Conductivity Properties of *in Situ* Produced BC/RGO Nanocomposite Films. The formation of BC/RGO nanocomposites through *in situ* fermentation process is likely to improve the electrical conductivity of films even in the presence of lower RGO loadings. Moreover, it was observed that the partially oxidized RGO sheets underwent *in situ* reductions during the fermentation (as confirmed from the XPS spectroscopy studies), which is expected to improve the conductivity values[41] of BC/RGO nanocomposites. Table 3 summarizes the measured electrical properties of BC/RGO films produced using different RGO concentrations used during *in situ* fermentation cultivation. The pristine BC films due to the absence of any conductive pathways show extremely low conductivity values of 3.6×10^{-5} S/cm, which is consistent with earlier published reports.[42] However, with lower RGO loadings (1 or 2 wt %) the electrical conductivity values were improved by 4−5 orders of magnitude. Interestingly, the conductivity achieved at RGO 3 wt %, was ∼7 orders of magnitude. The enhanced electrical conductivity at 3 wt % RGO loadings was probably due to the formation of percolated-structure (as discussed earlier Figure 7a), which creates a conductive network of interconnected RGO sheets in the BC matrix. The high conductivity value of 130 S/cm for

Table 3. Electrical Conductivities of the BC/RGO Nanocomposite Films Produced during the *in Situ* Fermentation Process

samples	sheet resistance (Ω)	thickness (μm)	specific resistivity (Ω·cm)	conductivity (S/cm)
BC	3.6×10^9	8.5	2.7×10^4	3.6×10^{-5}
BC_1RGO	1.098×10^3	10.1	1.098	9.1×10^{-1}
BC_2RGO	335.4	9.6	0.322	3.1
BC_3RGO	7.41	11.2	8.3×10^{-3}	112
BC_4RGO	6.17	12.3	7.6×10^{-3}	130
BC_5RGO	4.23	10.7	7.2×10^{-3}	138

BC/RGO films produced by *in situ* fermentation is comparable to the earlier reported BC nanocomposites containing polypyrrole,[43] carbon nanotubes,[8] or polyaniline[9] fabricated through chemical routes (as compared in Table S1). The measured conductivities of the films were sufficiently high for practical applications such as for the development of membrane electrode assemblies. The BC/RGO can also be used as free-standing films for electronic applications, due to their high flexibility. Electrical conductivity did not improve considerably with more than 3 wt % RGO addition which was assumed to be saturated concentration. The underlying mechanism for enhanced electrical conductivity and the presence of a 3D graphene network in nanocomposites by using the percolation threshold concentration were confirmed by using the power-law equation[44]

$$\phi_c = \phi_f(\rho - \rho_c)^n$$

where the parameters ϕ_c and ϕ_f represent the conductivity of fabricated nanocomposites and filler respectively, ρ refers to filler concentration, ρ_c represents concentrations of RGO at percolation threshold, and n represents the universal critical exponent. The universal critical exponent is an important parameter which indicates the type of percolation network depending on its values. As per classical percolation theory, $n \sim 1$ represents the presence of two-dimensional conductive systems, $n \sim 1.3$ signifies the formation of continuum networks, and $n \sim 1.6-2.0$ suggests a possible three-dimensional network of conductive micro/nanofillers.[45] From the log−log plot of electrical conductivity versus function of RGO content (Figure 7b), the percolation threshold of RGO was found to be ∼2.45 wt % or 1.08 vol %. The value of universal critical exponent (n) was determined from the slope of the logarithmic plot of conductivity versus ($\rho - \rho_c$), which was measured to be 2.1 suggesting the presence of three-dimensional type of percolated network. This discussion confirms the earlier assumption made from morphological investigations (Figure 4c) that the *in situ* fermentation of BC/RGO resulted in the formation of a three-dimensional percolated-network-like structures, which contained inter-cross-linked linkages of 2D graphene nanosheets resulting in a drastic increase in conductivity. To the best of our knowledge, the formation of percolated networks during the *in situ* fermentation process have never been reported in the literature. With a percolation threshold concentration of (ρ_c) ∼2.45 wt %, this finding is inline with earlier reports on graphene based nanocomposites processed through chemical modification routes.[46,47] It is noteworthy to mention that the formation of a percolated network during *in situ* fermentation is a sustainable route replacing the toxic chemical-based approaches on several other factors such as type, functionality, and aspect ratio of RGO nanosheets. All these factors need to be considered for further studies to thoroughly investigate the percolated network. Conclusively, the present study shows the formation of BC/RGO nanocomposites with kinetically controlled percolation-network through sustainable and greener routes of *in situ* fermentation which has promising applications as free-standing electrodes or paper-based supercapacitors.

■ CONCLUSIONS

A BC/RGO nanocomposite fabrication route based on an *in situ* fermentation approach with homogeneous dispersion and percolated-network formation was demonstrated in this study. The addition of RGO nanosheets at various concentrations to culture media was found to significantly affect the fermentation kinetic parameters. Maximum specific growth rate ($\mu_{\max}$) and yield coefficients were found to be improved considerably at an optimal RGO concentration of 3 wt %. It was observed that the physicochemical properties of produced BC/RGO nanocomposites were subjected to the fermentation condition and kinetics that provide a unique platform in tailoring the nanostructure properties depending on targeted applications. FTIR, XPS, and Raman spectroscopic studies reveal the presence of strong interactions between partially oxidized RGO sheets and BC fibers. The presence of intramolecular hydrogen-bonded forces and *in situ* reduction of RGO sheets due to hydrophobic interactions results in the formation of a three-dimensional entangled percolated network of BC nanofibers wrapped over RGO. Formation of such network of RGO in BC matrix was confirmed from classical percolation theory, based on the evaluation of mechanical and conductivity properties. The percolation threshold concentration was predicted to be ∼2−3 wt %, which is comparable with the values as obtained through chemical-based modification approaches. Furthermore, evaluation of molecular weight characteristics, crystallinity, surface area, and porosity of nanocomposites show a significant dependence on RGO as well as fermentation conditions. The resultant BC/RGO nanostructures with high flexibility displayed remarkable isotropic electrical conductivity of 112 S/cm and mechanical integrity with a tensile modulus of 151 MPa (at RGO loadings 3 wt %). Therefore, the present study investigates the kinetics of *in situ* fermentation process and evaluates the inherent properties of nanocomposites from an engineering perspective, which is required to address the challenges associated with its up-scaled production to meet the growing demands of technologies developed from renewable materials. BC/RGO nanocomposites produced through such a sustainable approach can be used in the development of scaffolds for tissue engineering with biosensing capabilities, free-standing films as electrodes or supercapacitors, air or water filter membranes, pollutant remediation, and as degradable patches for electro-responsive drug delivery systems. The present study can be extended in upconversion of agricultural waste or residues to value-added products based on the third-generation biorefinery concept, which will be explored in our subsequent studies.

■ ASSOCIATED CONTENT

Ⓢ Supporting Information

The Supporting Information is available free of charge on the ACS Publications website at DOI: 10.1021/acsabm.9b00581.

> TEM micrographs of functionalized RGO and electrical conductivity values from literature are compared with current study; E-supplementary data of this work can be found in an online version of the paper (PDF)

■ AUTHOR INFORMATION

Corresponding Authors

*Email: sandipbankar@gmail.com; sandip.bankar@aalto.fi (S.B.B.).
*Email: prodyutdhar3@gmail.com; dhar.prodyut.48a@st.kyoto-u.ac.jp (P.D.).

ORCID

Jarkko Etula: 0000-0002-6930-1165
Sandip Balasaheb Bankar: 0000-0003-0280-9949

Notes

The authors declare no competing financial interest.

ACKNOWLEDGMENTS

The authors are thankful to the Nanomicroscopy Center (Aalto-NMC), Aalto University, for SEM imaging facilities and Bioeconomy Facilities, Aalto University, for the XPS investigation. We are also grateful to Joseph Champbel for the XPS measurements.

ABBREVIATIONS

RGO = reduced graphene oxide
BC = bacterial cellulose
UTS = ultimate tensile strength
XPS = X-ray photoelectron spectroscopy
YM = Young's modulus

REFERENCES

(1) Moon, R. J.; Martini, A.; Nairn, J.; Simonsen, J.; Youngblood, J. Cellulose Nanomaterials Review: Structure, Properties and Nanocomposites. *Chem. Soc. Rev.* **2011**, *40* (7), 3941−3994.

(2) Dugan, J. M.; Gough, J. E.; Eichhorn, S. J. Bacterial Cellulose Scaffolds and Cellulose Nanowhiskers for Tissue Engineering. *Nanomedicine* **2013**, *8* (2), 287−298.

(3) Czaja, W.; Krystynowicz, A.; Bielecki, S.; Brown, R. M. Microbial Cellulose—the Natural Power to Heal Wounds. *Biomaterials* **2006**, *27* (2), 145−151.

(4) Fu, L.; Zhang, J.; Yang, G. Present Status and Applications of Bacterial Cellulose-Based Materials for Skin Tissue Repair. *Carbohydr. Polym.* **2013**, *92* (2), 1432−1442.

(5) Klemm, D.; Schumann, D.; Udhardt, U.; Marsch, S. Bacterial Synthesized Cellulose — Artificial Blood Vessels for Microsurgery. *Prog. Polym. Sci.* **2001**, *26* (9), 1561−1603.

(6) Stumpf, T. R.; Yang, X.; Zhang, J.; Cao, X. In Situ and Ex Situ Modifications of Bacterial Cellulose for Applications in Tissue Engineering. *Mater. Sci. Eng., C* **2018**, *82*, 372−383.

(7) Yang, Z.; Ren, L.; Jin, L.; Huang, L.; He, Y.; Tang, J.; Yang, W.; Wang, H. In situ Functionalization of Poly(m-Phenylenediamine) Nanoparticles on Bacterial Cellulose for Chromium Removal. *Chem. Eng. J.* **2018**, *344*, 441−452.

(8) Park, S.; Park, J.; Jo, I.; Cho, S.-P.; Sung, D.; Ryu, S.; Park, M.; Min, K.-A.; Kim, J.; Hong, S.; et al. In Situ Hybridization of Carbon Nanotubes with Bacterial Cellulose for Three-Dimensional Hybrid Bioscaffolds. *Biomaterials* **2015**, *58*, 93−102.

(9) Luo, H.; Dong, J.; Zhang, Y.; Li, G.; Guo, R.; Zuo, G.; Ye, M.; Wang, Z.; Yang, Z.; Wan, Y. Constructing 3D Bacterial Cellulose/Graphene/Polyaniline Nanocomposites by Novel Layer-by-Layer in Situ Culture toward Mechanically Robust and Highly Flexible Freestanding Electrodes for Supercapacitors. *Chem. Eng. J.* **2018**, *334*, 1148−1158.

(10) Luo, H.; Xie, J.; Wang, J.; Yao, F.; Yang, Z.; Wan, Y. Step-by-Step Self-Assembly of 2D Few-Layer Reduced Graphene Oxide into 3D Architecture of Bacterial Cellulose for a Robust, Ultralight, and Recyclable All-Carbon Absorbent. *Carbon* **2018**, *139*, 824−832.

(11) Boulanger, N.; Yu, V.; Hilke, M.; Toney, M. F.; Barbero, D. R. Graphene Induced Electrical Percolation Enables More Efficient Charge Transport at a Hybrid Organic Semiconductor/Graphene Interface. *Phys. Chem. Chem. Phys.* **2018**, *20* (6), 4422−4428.

(12) Nistal, A.; Garcia, E.; Pérez -Coll, D.; Prieto, C.; Belmonte, M.; Osendi, M. I.; Miranzo, P. Low Percolation Threshold in Highly Conducting Graphene Nanoplatelets/Glass Composite Coatings. *Carbon* **2018**, *139*, 556−563.

(13) Dhar, P.; Gaur, S. S.; Kumar, A.; Katiyar, V. Cellulose Nanocrystal Templated Graphene Nanoscrolls for High Performance Supercapacitors and Hydrogen Storage: An Experimental and Molecular Simulation Study. *Sci. Rep.* **2018**, *8* (1), 3886.

(14) Reiniati, I.; Hrymak, A. N.; Margaritis, A. Kinetics of Cell Growth and Crystalline Nanocellulose Production by Komagataeibacter Xylinus. *Biochem. Eng. J.* **2017**, *127*, 21−31.

(15) Chao, Y.; Mitarai, M.; Sugano, Y.; Shoda, M. Effect of Addition of Water-Soluble Polysaccharides on Bacterial Cellulose Production in a 50-L Airlift Reactor. *Biotechnol. Prog.* **2001**, *17* (4), 781−785.

(16) Shen, X.; Ji, Y.; Wang, D.; Yang, Q. Solubility of a High Molecular-Weight Bacterial Cellulose in Lithium Chloride/N,N-Dimethylacetamide Solution. *J. Macromol. Sci., Part B: Phys.* **2010**, *49* (5), 1012−1018.

(17) Borrega, M.; Tolonen, L. K.; Bardot, F.; Testova, L.; Sixta, H. Potential of Hot Water Extraction of Birch Wood to Produce High-Purity Dissolving Pulp after Alkaline Pulping. *Bioresour. Technol.* **2013**, *135*, 665−671.

(18) Johnson, D. W.; Dobson, B. P.; Coleman, K. S. A Manufacturing Perspective on Graphene Dispersions. *Curr. Opin. Colloid Interface Sci.* **2015**, *20* (5), 367−382.

(19) Mohammadkazemi, F.; Azin, M.; Ashori, A. Production of Bacterial Cellulose Using Different Carbon Sources and Culture Media. *Carbohydr. Polym.* **2015**, *117*, 518−523.

(20) Żywicka, A.; Fijałkowski, K.; Junka, A. F.; Grzesiak, J.; El Fray, M. Modification of Bacterial Cellulose with Quaternary Ammonium Compounds Based on Fatty Acids and Amino Acids and the Effect on Antimicrobial Activity. *Biomacromolecules* **2018**, *19* (5), 1528−1538.

(21) Luo, H.; Dong, J.; Yao, F.; Yang, Z.; Li, W.; Wang, J.; Xu, X.; Hu, J.; Wan, Y. Layer-by-Layer Assembled Bacterial Cellulose/Graphene Oxide Hydrogels with Extremely Enhanced Mechanical Properties. *Nano-Micro Lett.* **2018**, *10* (3), 42.

(22) Casaburi, A.; Montoya Rojo, Ú.; Cerrutti, P.; Vázquez, A.; Foresti, M. L. Carboxymethyl Cellulose with Tailored Degree of Substitution Obtained from Bacterial Cellulose. *Food Hydrocolloids* **2018**, *75*, 147−156.

(23) Luo, H.; Dong, J.; Xu, X.; Wang, J.; Yang, Z.; Wan, Y. Exploring Excellent Dispersion of Graphene Nanosheets in Three-Dimensional Bacterial Cellulose for Ultra-Strong Nanocomposite Hydrogels. *Composites, Part A* **2018**, *109*, 290−297.

(24) Nandgaonkar, A. G.; Wang, Q.; Fu, K.; Krause, W. E.; Wei, Q.; Gorga, R.; Lucia, L. A. A One-Pot Biosynthesis of Reduced Graphene Oxide (RGO)/Bacterial Cellulose (BC) Nanocomposites. *Green Chem.* **2014**, *16* (6), 3195−3201.

(25) Tsouko, E.; Kourmentza, C.; Ladakis, D.; Kopsahelis, N.; Mandala, I.; Papanikolaou, S.; Paloukis, F.; Alves, V.; Koutinas, A. Bacterial Cellulose Production from Industrial Waste and By-Product Streams. *Int. J. Mol. Sci.* **2015**, *16* (7), 14832−14849.

(26) Duan, J.; Gong, S.; Gao, Y.; Xie, X.; Jiang, L.; Cheng, Q. Bioinspired Ternary Artificial Nacre Nanocomposites Based on Reduced Graphene Oxide and Nanofibrillar Cellulose. *ACS Appl. Mater. Interfaces* **2016**, *8* (16), 10545−10550.

(27) Wang, J.; Cheng, Q.; Lin, L.; Jiang, L. Synergistic Toughening of Bioinspired Poly(Vinyl Alcohol)−Clay−Nanofibrillar Cellulose Artificial Nacre. *ACS Nano* **2014**, *8* (3), 2739−2745.

(28) Farhadi-Khouzani, M.; Schütz, C.; Durak, G. M.; Fornell, J.; Sort, J.; Salazar-Alvarez, G.; Bergström, L.; Gebauer, D. A $CaCO_3$/Nanocellulose-Based Bioinspired Nacre-like Material. *J. Mater. Chem. A* **2017**, *5* (31), 16128−33.

(29) Zhu, W.; Li, W.; He, Y.; Duan, T. In situ Biopreparation of Biocompatible Bacterial Cellulose/Graphene Oxide Composites Pellets. *Appl. Surf. Sci.* **2015**, *338*, 22−26.

(30) Roman, M.; Winter, W. T. Effect of Sulfate Groups from Sulfuric Acid Hydrolysis on the Thermal Degradation Behavior of Bacterial Cellulose. *Biomacromolecules* **2004**, *5* (5), 1671−1677.

(31) Guo, Y.; Xu, G.; Yang, X.; Ruan, K.; Ma, T.; Zhang, Q.; Gu, J.; Wu, Y.; Liu, H.; Guo, Z. Significantly Enhanced and Precisely Modeled Thermal Conductivity in Polyimide Nanocomposites with Chemically Modified Graphene via in Situ Polymerization and

Electrospinning-Hot Press Technology. *J. Mater. Chem. C* **2018**, *6* (12), 3004−3015.

(32) Tian, M.; Qu, L.; Zhang, X.; Zhang, K.; Zhu, S.; Guo, X.; Han, G.; Tang, X.; Sun, Y. Enhanced Mechanical and Thermal Properties of Regenerated Cellulose/Graphene Composite Fibers. *Carbohydr. Polym.* **2014**, *111*, 456−462.

(33) Hervy, M.; Bock, F.; Lee, K.-Y. Thinner and Better: (Ultra-)Low Grammage Bacterial Cellulose Nanopaper-Reinforced Polylactide Composite Laminates. *Compos. Sci. Technol.* **2018**, *167*, 126−133.

(34) Chen, S.-Q.; Lopez-Sanchez, P.; Wang, D.; Mikkelsen, D.; Gidley, M. J. Mechanical Properties of Bacterial Cellulose Synthesised by Diverse Strains of the Genus Komagataeibacter. *Food Hydrocolloids* **2018**, *81*, 87−95.

(35) Dhar, P.; Tarafder, D.; Kumar, A.; Katiyar, V. Effect of Cellulose Nanocrystal Polymorphs on Mechanical, Barrier and Thermal Properties of Poly(Lactic Acid) Based Bionanocomposites. *RSC Adv.* **2015**, *5* (74), 60426−60440.

(36) Ouali, N.; Perez, J. C. Elastic, Viscoelastic and Plastic Behavior of Multiphase Polymer Blends. *Plast. Rubber Compos. Process. Appl.* **1991**, *16*, 55−60.

(37) Chen, Q.; Gong, S.; Moll, J.; Zhao, D.; Kumar, S. K.; Colby, R. H. Mechanical Reinforcement of Polymer Nanocomposites from Percolation of a Nanoparticle Network. *ACS Macro Lett.* **2015**, *4* (4), 398−402.

(38) Lee, K.-Y.; Aitomäki, Y.; Berglund, L. A.; Oksman, K.; Bismarck, A. On the Use of Nanocellulose as Reinforcement in Polymer Matrix Composites. *Compos. Sci. Technol.* **2014**, *105*, 15−27.

(39) Dalmas, F.; Cavaillé, J.-Y.; Gauthier, C.; Chazeau, L.; Dendievel, R. Viscoelastic Behavior and Electrical Properties of Flexible Nanofiber Filled Polymer Nanocomposites. Influence of Processing Conditions. *Compos. Sci. Technol.* **2007**, *67* (5), 829−839.

(40) De Gennes, P.G. On a Relation between Percolation Theory and the Elasticity of Gels. *J. Phys., Lett.* **1976**, *37* (1), 1−2.

(41) Ccorahua, R.; Troncoso, O. P.; Rodriguez, S.; Lopez, D.; Torres, F. G. Hydrazine Treatment Improves Conductivity of Bacterial Cellulose/Graphene Nanocomposites Obtained by a Novel Processing Method. *Carbohydr. Polym.* **2017**, *171*, 68−76.

(42) Erbas Kiziltas, E.; Kiziltas, A.; Rhodes, K.; Emanetoglu, N. W.; Blumentritt, M.; Gardner, D. J. Electrically Conductive Nano Graphite-Filled Bacterial Cellulose Composites. *Carbohydr. Polym.* **2016**, *136*, 1144−1151.

(43) Liu, Y.; Zhou, J.; Tang, J.; Tang, W. Three-Dimensional, Chemically Bonded Polypyrrole/Bacterial Cellulose/Graphene Composites for High-Performance Supercapacitors. *Chem. Mater.* **2015**, *27* (20), 7034−7041.

(44) Wang, Z.; Shen, X.; Han, N. M.; Liu, X.; Wu, Y.; Ye, W.; Kim, J.-K. Ultralow Electrical Percolation in Graphene Aerogel/Epoxy Composites. *Chem. Mater.* **2016**, *28* (18), 6731−6741.

(45) Nassira, H.; Sánchez-Ferrer, A.; Adamcik, J.; Handschin, S.; Mahdavi, H.; Qazvini, N. T.; Mezzenga, R. Gelatin−Graphene Nanocomposites with Ultralow Electrical Percolation Threshold. *Adv. Mater.* **2016**, *28* (32), 6914−6920.

(46) Shtein, M.; Nadiv, R.; Buzaglo, M.; Kahil, K.; Regev, O. Thermally Conductive Graphene-Polymer Composites: Size, Percolation, and Synergy Effects. *Chem. Mater.* **2015**, *27* (6), 2100−2106.

(47) Stankovich, S.; Dikin, D. A.; Dommett, G. H. B.; Kohlhaas, K. M.; Zimney, E. J.; Stach, E. A.; Piner, R. D.; Nguyen, S. T.; Ruoff, R. S. Graphene-Based Composite Materials. *Nature* **2006**, *442* (7100), 282−286.